Research Article

Model for Predicting the Head Shape of a Taylor Bubble Rising through Stagnant Liquids in a Vertical Tube

Boonchai Lertnuwat *
Department of Mechanical Engineering, Chulalongkorn University,
Patumwan, Bangkok 10330 Thailand.

Abstract

Dumitresku's model is a classic model for predicting the shape of a Taylor bubble head. Since the model consists of two equations, there is a discontinuity in predicting Taylor bubble surfaces when two equations are switched. A proposed model is derived from Euler's equation and based on the Dumitresku's model. It can predict the whole shape of a Taylor bubble head, similar to the Dumitresku's model. However, this model reduces the discontinuity which regularly occurs in the Dumitresku's model due to the equations switching. Similarities between the Dumitresku's model and the proposed model are investigated through a numerical simulation of flow fields around a Taylor bubble head. Simulation results show that the geometric and kinematic similarities between the two models are extremely ensured while the dynamic similarity is acceptably ensured with less confidence. However, the proposed model can partially reduce the discontinuities in the simulation results as desired.

Keywords: Computation; Dumitresku's model; Euler's equation; Similarity; Taylor bubble.

1. Introduction

An interesting pattern of two-phase gas-liquid flows in pipes is slug flow which is characterized by a succession of liquid slugs, separated by elongation bubbles (the so called Taylor bubbles) rising upward, as shown in Fig. 1(a). The flow pattern is usually observed in engineering works. Many research topics focus on studying slug flow phenomena, for instance, the pressure drop across a slug unit [1,2], the flow field around a Taylor bubble [3-5] and the dynamics of entrained dispersed bubbles [6]. The shape of a Taylor bubble head is an interesting topic because it influences the flow field and the pressure drop around the Taylor bubbles. Nogueira *et al.* [7] predicted the shape of Taylor bubble head by employing a classic model of Dumitrescu [8]. Dumitrescu's model is derived from the theory of potential flow and is used for predicting the shape of Taylor bubble heads in a stagnant liquid pipe based on 2 equations, namely, a circle radius equation $3/4R_p$ and a nonlinear-polynomial equation as shown with Eq. (1) and Eq. (2), respectively:

$$R_b = R_p\left[\frac{\Delta z}{R_p}\left(\frac{3}{2}-\frac{\Delta z}{R_p}\right)\right]^{\frac{1}{2}} \text{ when } \Delta z \le 0.5R_p\,, \quad (1)$$

$$R_b = R_p\left[1-Fr_D\left(\frac{R_p}{\Delta z}\right)^{\frac{1}{2}}\right]^{\frac{1}{2}} \text{ when } \Delta z > 0.5R_p\,, \quad (2)$$

where

$$\Delta z = z_{nose} - z \text{ and} \quad (3)$$

$$Fr_D = 0.351\,. \quad (4)$$

***Correspondence** : Boonchai.L@Chula.ac.th

It is apparent that there is a discontinuity in the shape of a Taylor bubble at $\Delta z = 0.5R_p$ when Eq. (1) is switched to Eq. (2). This disagrees with reality. In addition, splitting the shape of a Taylor bubble head into 2 parts is rather difficult for researchers who want to study the change of Taylor bubble shape due to some influences of the flow field around the Taylor bubble, e.g., pipe diameter, viscosity and surface tension. Consequently, the objective of this work is to derive a model that can predict the whole shape of a Taylor bubble head, similar to the Dumitresku's model, without switching equations.

2. Model derivation

Generally, the velocity field of the flows around a Taylor bubble is considered with respect to the bubble nose as shown in Fig. 1(b). As a result of the symmetry around the pipe centerline, only the right side of the flow field in Fig. 1(b) is considered as shown in Fig.2. If the streamline adjacent to the outside surface of the Taylor bubble is drawn as illustrated in Fig. 2, we will find that the liquid flows toward the Taylor bubble and that there is a stagnation point at the Taylor bubble nose. The liquid finally flows along the free surface of the Taylor bubble. Because the flow along the Taylor bubble surface is incompressible and inviscid, it can be governed by the Euler's equation:

$$\rho_l \frac{D\vec{V}}{Dt} = \rho_l \vec{g} - \vec{\nabla} p_l \,. \qquad (5)$$

Since the Euler's equation is applied along the streamline over the Taylor bubble, it turns out to be

$$\rho_l \left(\frac{\partial V}{\partial t} + V \frac{\partial V}{\partial s} \right) = -\rho_l g \frac{\partial z}{\partial s} - \frac{\partial p_l}{\partial s} \,. \qquad (6)$$

Generally, the effect of tension and normal stress on the Taylor bubble surface is negligibly small. This leads to static pressure that is constant along the streamline, that is $p_l = p_{nose}$ or $\partial p_l / \partial s = 0$. Moreover, if the flow is steady, Eq. (6) will become

$$V \partial V = -g \partial z \,. \qquad (7)$$

Integrating Eq. (7) from the Taylor bubble nose results in

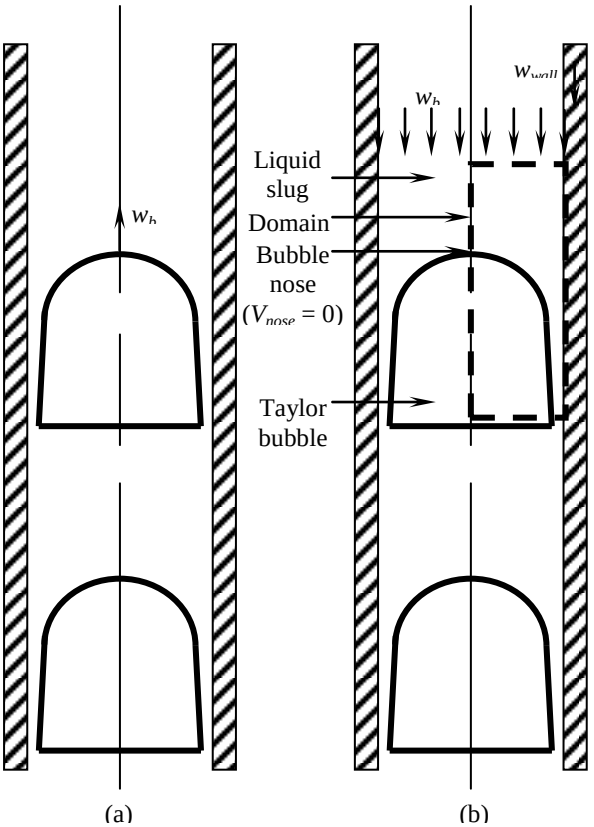

Fig.1. Schematic diagram of slug flow (a) with respect to pipe wall (b) with respect to Taylor bubble nose.

$$V_l^2 - V_{nose}^2 = 2g\Delta z \,, \qquad (8)$$

or

$$\beta_l \bar{w}_l^2 - \beta_{nose} \bar{w}_{nose}^2 = 2g\Delta z \,, \qquad (9)$$

where

$$\beta = \left(V / \bar{w} \right)^2 . \qquad (10)$$

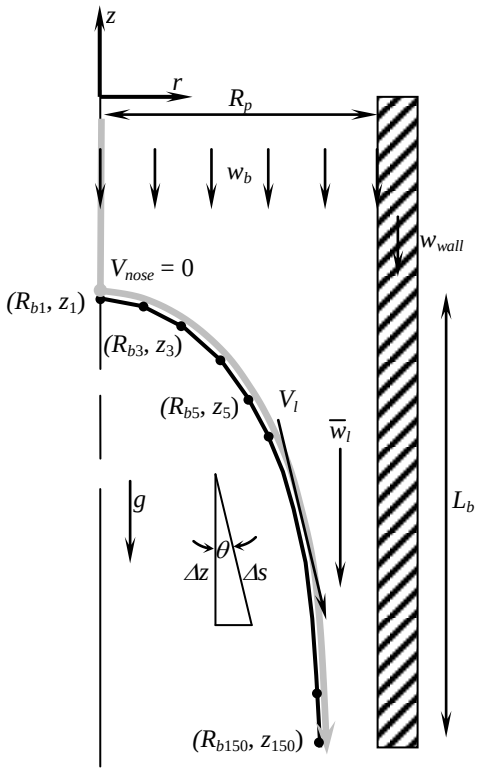

Fig.2. Schematic diagram of the streamline of the flow on the outside surface of a Taylor bubble created by 150 coordinate points which are evenly distributed.

In case of steady flow, the mass flux, across each pipe cross-sectional area, must be constant. And it must be equal to the mass flux across the inlet sectional area, i.e.,

$$\rho_l \overline{w}_l \pi\left(R_p^2 - R_b^2\right) = \rho_l w_b \pi\left(R_p^2\right)$$

or

$$\overline{w}_l = \left[R_p^2 \Big/ \left(R_p^2 - R_b^2\right)\right] w_b \,. \qquad (11)$$

Substituting Eq. (11) into Eq. (9) yields

$$\beta_l \left[R_p^2 \Big/ \left(R_p^2 - R_b^2\right)\right]^2 w_b^2 - \beta_{nose} \left[R_p^2 \Big/ \left(R_p^2 - R_{nose}^2\right)\right]^2 w_b^2 = 2g\Delta z \qquad (12)$$

R_{nose}, which is R_{b1} in Fig. 2, must be zero. Therefore, Eq. (12) becomes

$$R_b = R_p \left[1 - \left(\frac{\beta_l w_b^2}{2g\Delta z + \beta_{nose} w_b^2}\right)^{\frac{1}{2}}\right]^{\frac{1}{2}} . \qquad (13)$$

Since the Taylor bubble nose is a stagnation point as shown in Fig. 2, the nose velocity (V_{nose}) must be zero. This results in $\beta_{nose} = 0$, in accordance with Eq. (10). Hence, both Eq. (13) can be reduced to

$$R_b = R_p \left[1 - \left(\frac{\beta_l w_b^2}{2g\Delta z}\right)^{\frac{1}{2}}\right]^{\frac{1}{2}} . \qquad (14)$$

Eq. (14) is potentially applicable because it will turn out to be Eq. (2) when $\beta_l = 1$.

Although Eq. (14) is theoretically correct, there is a singularity at $\Delta z = 0$. Employing a small constant (δ) avoids the problem and improves Eq. (14). This yields

$$R_b = R_p \left[1 - \left(\frac{\beta w_b^2 + \delta}{2g\Delta z + \delta}\right)^{\frac{1}{2}}\right]^{\frac{1}{2}} . \qquad (15)$$

Herein, δ is assigned to be 10^{-38}.

The variable β_l is determined by Eq. (1) and Eq. (2) so that the proposed model will be similar to the Dumitresku model under a set of appropriate parameters. Because Froude number is employed in Eq. (2), it must be set properly. Hayashi [9] proposed that Froude number is predicted with

$$Fr = \left(\frac{0.01}{0.0816 + Re^{-1}}\right)^{\frac{1}{2}} \qquad (16)$$

where

$$Re = \rho_l w_b D_p / \mu_l \,, \qquad (17)$$

$$w_b = Fr\sqrt{2gR_p} \qquad (18)$$

when Eötvös number (Eo) is larger than 100. Nigmatulin and Bonetto [10] suggested that Froude number should be 0.351 in Eq. (2). This means that Re must be as large as possible, resulting in the largest possible D_p.

Because Nogueira *et al.* [7] stated that the Dumitrescu's model predicted the shape of Taylor bubbles, agreeing well with the experimental data of Mao *et al.* [11] for air-water systems, an air-water slug flow rising in stagnant water is firstly selected for this study. Therefore, a pipe with a diameter of 0.1m is used in this study since air-water slug flows rising in stagnant water have generally been observed only in pipes with a diameter not larger than 0.1m [12-14].

The length of a Taylor bubble (L_b) is another important parameter. In experiments [11, 15, 16], the length of a Taylor bubble varies from $4\,D_p$ to $30\,D_p$, approximately. The length of the Taylor bubble exploited in this study is set to be $5\,D_p$ (L_b=0.500m) so that the Taylor bubble head is specifically focused. After setting R_p=0.050m and L_b =0.500m, the curve of the Taylor bubble head will be created by Eq. (1) and Eq. (2) with 150 points of coordinates as illustrated in Fig. 2. The coordinate points are distributed along the bubble surface at an approximately equal interval. Finally, it is found that these points of coordinates are well fitted with Eq. (14) and β_l as predicted by

$$\beta_l = a_1\left(1-e^{a_2\Delta z}\right) \qquad (19)$$

in which $a_1 = 1.067$ and $a_2 = -152.7$.

3. Computational Setup

The proposed model is computationally investigated in comparison to the Dumitresku's model in this section. The computational domain is the space confined in the dashed box shown in Fig. 1(b). The domain occupies only the right side of the pipe due to the symmetry along the pipe centerline. The pipe radius (R_p) is 0.050m, and the Taylor bubble length (L_b) is $5\,D_p$ (=0.500m). The slug length (L_s) in front of the Taylor bubble (indicated in Fig. 3) must be long enough to prevent the inlet boundary condition from the influence of flow reversal around the Taylor bubble nose. Shemer [17] stated that the flow reversal approximately occurs at $0.5\,D_p$ above the bubble trip. Hout [18] reported that large vortices decayed and that the flow tended to become stagnant again approximately $2\,D_p$ behind the bubble tail. Nevertheless, the stable slug length, as found in experiments, is between 4-20 D_p [15, 16]. In this investigation, the slug length (L_s) is set to be $15\,D_p$ (= 1.500m), which is sufficiently long. The computational program is developed from the program code (CAFFA.F) provided by Ferziger [19]. The standard cylindrical k-ε model is employed. And the implicit pressure-correction method on the finite volume framework with the second order spatial accuracy is applied in the code.

As illustrated in Fig. 3, 31 gridlines are placed on r-axis. There are 2 sets of gridline on z-axis: 166 gridlines are drawn from the pipe centerline, and 150 gridlines are drawn from the Taylor bubble surface. A velocity inlet boundary condition is posed at the top of the computational domain with a fixed velocity (w_b=0.347m/s). A fixed outlet mass flux condition is posed on the bottom of the domain ($\dot{m}_{out} = \dot{m}_{in}$). A no-slip condition with a wall function is posed along the pipe wall on the right side of the domain with a fixed wall velocity (w_{wall}=0.347m/s). A symmetry boundary condition is posed on the left side of the domain. The fluid is water of which density and viscosity are respectively 997.0 kg/m^3 and 8.910×10^{-4}Pa-s.

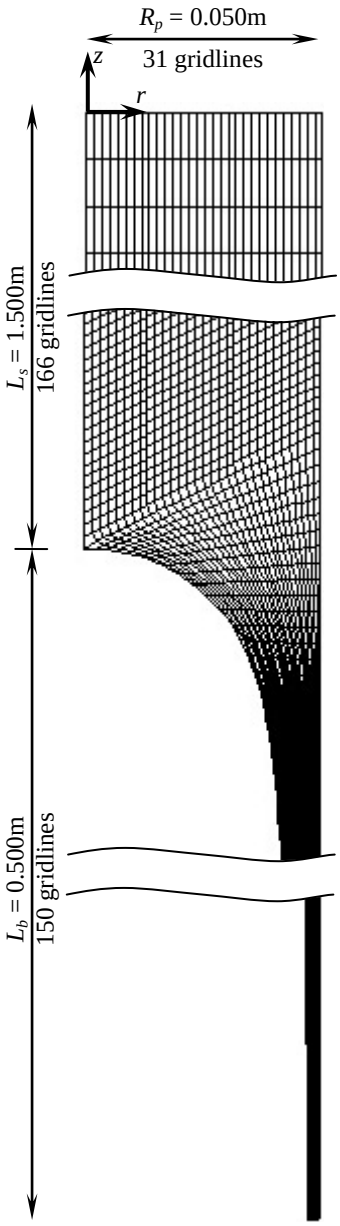

Fig.3. Computational domain and exploited grid.

4. Results and Discussion

First, the comparison of the flow fields over the Taylor bubble surface predicted using two different models is discussed. Since the flow fields are severely developed within the region around the Taylor bubble head, Fig. 4 shows only the flow fields in the region for a better comparison. According to Fig. 4, the two simulated flow fields, shown with vector plots, are similar. Both velocity profiles similarly develop from a uniform flow (on the top of the figure) to become a non-uniform flow with a stagnation point at the Taylor bubble nose (z = -1.500m). Then, both flows are faster within the narrow gap between the pipe wall and the Taylor bubble surface to maintain a constant mass flux. While the static pressure distributions, shown with the contour lines, rapidly increase within the upper half of both flow fields due to hydrostatic pressure (gravity). Then, there is a low variation in the static pressure distributions within the lower half of both flow fields due to the balance between hydrostatic pressure and dynamic pressure.

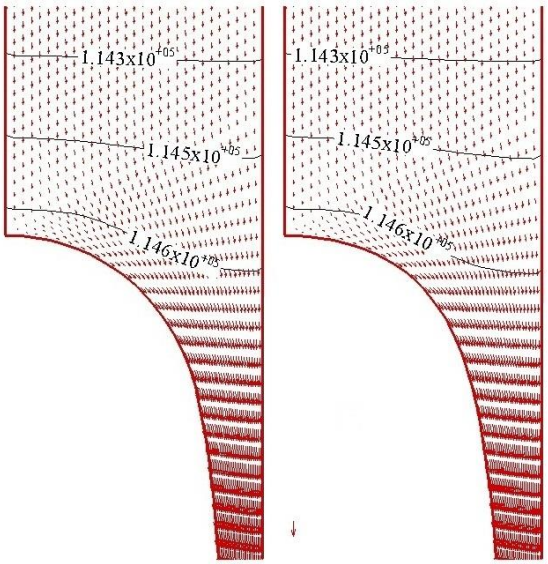

Fig.4. Comparison of velocity and pressure fields around the Taylor bubble head computed from (a) the Dumitresku's model and (b) the proposed model (the unit of the contour lines is Pa).

The comparison is further explored by investigating three levels of flow similarity on the Taylor bubble surface, namely, geometric, kinematic and dynamic similarities. The geometric similarity can be investigated as shown in Fig. 5. The figure shows the

comparison of Taylor bubble surfaces predicted based on the two models. It is obvious that the Taylor bubble surface predicted based on the proposed models fits well with that predicted based on the Dumitresku's model. However, as shown in Fig. 6, some discrepancy will be found in the region around the head of the Taylor bubble if the region is magnified. The discrepancy can be used for calculating a correlation coefficient (r) [20] so that the investigation is easier. In this case, the correlation coefficient (r) is 0.9994. This means that the discrepancy is very small since the correlation coefficient (r) is very close to unity. Therefore, the geometric similarity is ensured.

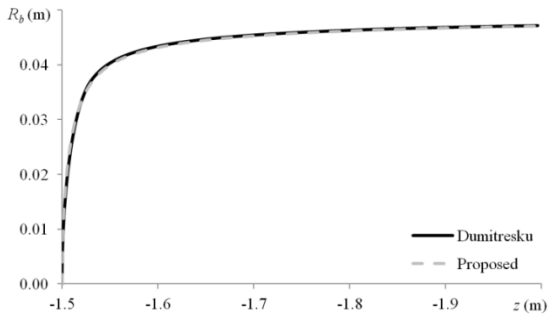

Fig.5. Comparison of Taylor bubble shapes predicted based on the Dumitresku's model and the proposed model.

The kinematic similarity can be investigated as shown in Fig. 7 and Fig. 8, which show the comparisons of velocity components on the Taylor bubble surfaces. Fig.7 reveals that the velocity components on z-axis continuously decrease from zero with an abrupt change approximately at z =-1.525m (Δz =0.025m) for both models. According to Eq. (1) and Eq. (2), the position Δz =0.025m is the position where the switching of these two equations occurs ($\Delta z = 0.5R_p$). This is likely to be the reason why there is an abrupt change in both curves in Fig. 7. However, it is quite doubtful because there is no obvious discontinuity in Fig. 6. This may confirm that the velocity component on the z-axis is very sensitive to Taylor bubble shapes and discontinuity must be diminished to obtain better result. The discrepancy between two curves in Fig. 7 is small at first but gradually increases along the Taylor bubble length. The correlation coefficient (r) in Fig. 7 is 0.9970.

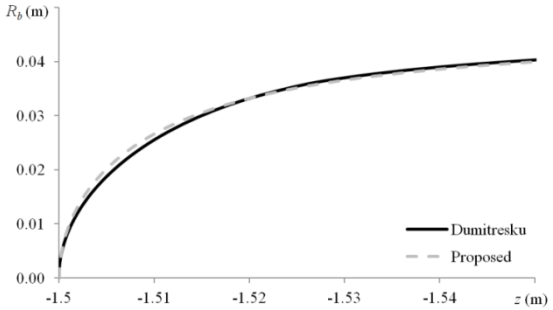

Fig.6. Comparison of the shapes of Taylor bubble predicted from the Dumitresku's model and the proposed model (within the region close to Taylor bubble nose).

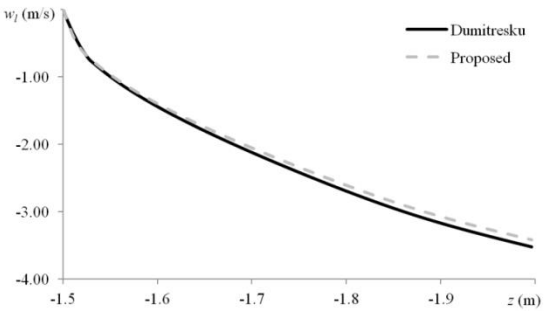

Fig.7. Comparison of velocity component on z-axis along Taylor bubble surfaces predicted based on the Dumitresku's model and the proposed model.

Fig. 8 reveals that the velocity components on r-axis first increase from zero, then decrease approximately at z = -1.510m (Δz =0.010m) for both models. There is, indeed, an unsmooth change in the curve of the Dumitresku's model as indicated by an arrow at $\Delta z = 0.5R_p$. But the change is not as obvious as that in Fig. 7. The discrepancy between these two curves can be used to calculate the correlation coefficient (r) which is 0.9962. Because both Fig. 7 and Fig. 8 give

the correlation coefficient (r) in the same order of magnitude which is very close to unity, the kinematic similarity can be ensured.

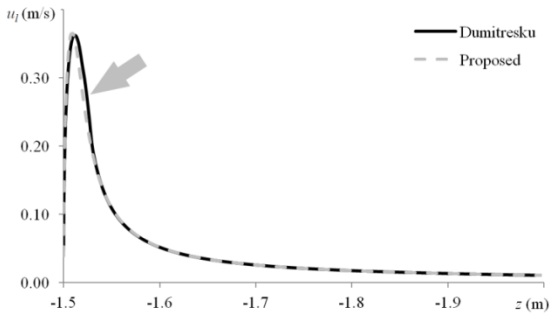

Fig.8. Comparison of velocity component on r-axis along Taylor bubble surfaces predicted based on the Dumitresku's model and the proposed model.

The dynamic similarity is the similarity of forces acting on the Taylor bubble surface. Theoretically, shear on any free surfaces is equal to zero. Although there is some shear in practice, it is negligibly small compared to normal force. The normal force on the Taylor bubble surface is a result of two contributions, namely, normal stress and pressure. Since normal stress is much smaller than pressure in the case of incompressible flows. Comparison between pressure distributions on the Taylor bubble surface is, thus, sufficient for ensuring the dynamic similarity. Fig. 9 shows the pressure distributions on the two Taylor bubble surfaces. It is apparent that there is some discrepancy although both curves similarly develop. The correlation coefficient (r) calculated from these two curves is 0.9324. The magnitude of the correlation coefficient (r) is rather less than those obtained from Fig. 5, Fig. 7 and Fig. 8. Nonetheless, it is still close to unity, i.e., it can ensure the dynamic similarity with sufficiently high confidence. Once again, an abrupt change is found in both curves. But the proposed model gives a smaller abrupt change. This may be because there is no switching of equations as in the Dumitresku's model.

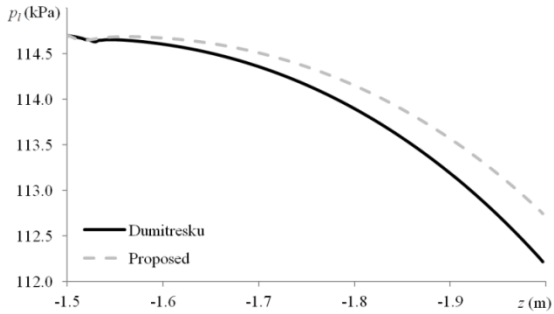

Fig.9. Comparison of static pressure along Taylor bubble surfaces predicted based on the Dumitresku's model and the proposed model.

Besides water, some other fluids, of which Fr equals to 0.351 but Re differs, are also employed to investigate the similarities. Table 1 shows that the r of p_l is the least when it is compared to the r of R_b, w_l and u_l for each fluid. However, the minimum r of p_l is 0.9324 which is still sufficiently high.

Table1. Properties [21] and correlation coefficients of R_b, w_l, u_l and p_l for used fluids.

Liquids	ρ_l kg/m^3	μ_l cP	σ g/m^2	$\rho_l^2 g D_p^3/\mu_l^2$	Re	Eo	Fr	r			
								R_b	w_l	u_l	p_l
Water	997	0.891	72.0	1.2×10^{10}	38900	1360	0.351	0.9994	0.9970	0.9962	0.9324
Ethylene glycol	1113	19.9	47.5	3.1×10^{7}	1940	2300	0.351	0.9994	0.9970	0.9965	0.9863
58% Sucrose solution	1272	40.5	76	9.7×10^{6}	1090	1640	0.351	0.9994	0.9970	0.9965	0.9882
Tellus oil	864	52	31	2.7×10^{6}	578	2730	0.351	0.9994	0.9970	0.9966	0.9895
90% Diluted glycerol	1234	154	64.8	6.3×10^{5}	279	1870	0.351	0.9994	0.9970	0.9967	0.9905

5. Conclusions

5.1 A model which can predict the whole shape of a Taylor bubble head, similar to the Dumitresku's model, is derived from the Euler's equation and based on the Dumitresku's model so that there is no equation switching. The proposed model consists of Eq. (15) and Eq. (19) for L_b =0.500m.

5.2 We found that the geometric and kinematic similarities between the Dumitresku's model and the proposed model are ensured with very high correlation coefficient (r) while the dynamic similarity is also ensured but with a smaller correlation coefficient. The minimum value for r is 0.9324 (the r of p_l for water).

5.3 Approximately at $\Delta z = 0.5R_p$, there is an abrupt change in the distribution curves of R_b, w_l, u_l and p_l which are obtained based on both the Dumitresku's model and the proposed model. But the abrupt changes are more pronounced in the curves obtained from the Dumitresku's model. This may be because of the switching between Eq. (1) and Eq. (2) in the model. Hence, it can be concluded that the proposed model can partially reduce the discontinuity.

5.4 The proposed model is derived by assuming that there is no heat transfer across the bubble surface and that the surface of the bubbles is symmetrical along the pipe centerline. Users must bear in mind these restrictions.

5.5 The void fraction is generally an important parameter in two-phase flows. With this proposed model, it can be calculated as follows:

Void fraction $(f) = V_{bubble}/V_{total}$

where $V_{bubble} = \int_{z_{nose}}^{z_{nose}+L_b} \pi R_b^2 dz$ and

$V_{Total} = \pi R_P^2 (L_s + L_b)$.

5.6 A limitation of applying the proposed model is found when it is exploited to predict the shape of Taylor bubble head with very small Δz, i.e., when $0 < \Delta z < 0.001 R_p$ in which case the proposed model will give imaginary numbers. Nevertheless, interpolation can be used in this narrow interval with an acceptable error.

Nomenclature

Characters

D : Pipe diameter

Eo : Eötvös number; $(\rho_l - \rho_g) g D_p^2 / \sigma$

Fr : Froude number; $w_b / \sqrt{2gR_p}$

g : Gravity acceleration

k : Turbulent kinetic energy

L : Length

p : Static pressure

R : Radius

r : Location on r-axis or Correlation coefficient

Re : Reynolds number; $\rho_l w_b D_p / \mu_l$

s : Surface

u : Velocity component on r-axis

V : Total velocity

w : Velocity component on z-axis

z : Location on z-axis

Symbols

β : Velocity ratio squared; $\beta = (V/\bar{w})^2$

δ : A small constant

ε : Dissipation

μ : Viscosity

ρ : Density

σ : Tension

Superscripts and Subscripts

b : Taylor bubble

D : Dumitresku

g : Gas

l : Liquid

nose : Taylor bubble nose

p : Pipe

s : Slug

wall : Pipe wall

6. References

[1] Woehl, P. and Cerro, R.L., Pressure Drop in Monolith Reactors, Catalysis Today, Vol.69, pp. 171-174, 2001.

[2] Mishima, K. and Hibiki, T., Some Characteristics of Air-Water Two-Phase Flow in Small Diameter Vertical Tubes, Int. J. Multiphase Flow, Vol.22, No.4, pp.703-712, 1996.

[3] Hout, R.V., Gulitski, A., Barnea, D. and Shemer, L., Experimental Investigation of the Velocity Field Induced by a Taylor Bubble Rising in Stagnant Water, Int. J. Multiphase Flow, Vol.28, No.4, pp.579-596, 2002.

[4] Mi, Y., Ishii, M. and Tsoukalas, L.H., Investigation of Vertical Slug Flow with Advanced Two-Phase Flow Instrumentation, Nuclear Engineering and Design, Vol.204, pp.69–85, 2001.

[5] Lertnuwat, B. and Bunyajitradulya, A., Effects of Interfacial Shear Condition and Trailing-Corner Radius on the Wake Vortex of a Bubble, Nuclear Engineering and Design, Vol.237, No. 14, pp.1526-1533, 2007.

[6] Lertnuwat, B., The Trajectory of Dispersed Bubbles around a Taylor Bubble Nose, Thammasat Int. J. Sc. Tech., Vol.11, No. 4, pp.56-64, 2006.

[7] Nogueira, S., Riethmuler, M.L., Campos, J.B.L.M. and Pinto, A.M.F.R., Flow in the nose region and annular film around a Taylor bubble rising through vertical columns of stagnant and flowing Newtonian liquids, Chemical Engineering Science, Vol.61, pp.845-857, 2006.

[8] Dumitrescu, D.T., Strömung an einer Luftblase im Senkrechten Rohr, Zeitschrift fur Angewandte Mathematik und Mechanik, Vol.23, pp.139–149, 1943.

[9] Hayashi, K., Kurimoto, R. and Tomiyama, A., Terminal velocity of a Taylor drop in a vertical pipe, Int. J. Multiphase Flow, Vol.37, pp.241-251, 2011.

[10] Nigmatulin, T.R. and Bonetto, F.J., Shape of Taylor Bubbles in Vertical Tubes, Int. Comm. Heat Mass Transfer, Vol.24, No.8, pp.1177-1185, 1997.

[11] Mao, Z-S. and Dukler, A.E., The Motion of Taylor Bubbles in Vertical Tubes-II. Experimental Data and Simulations for Laminar and Turbulent Flow, Chemical Engineering Science, Vol.46, No.8, pp.2055-2064, 1991.

[12] Kytömaa, H.K. and Brennen, C.E., Small Amplitude Kinematic Wave Propagation in Two-Component Media, Int. J. Multiphase Flow, Vol.17, No.1, pp.13-26, 1991.

[13] Cheng, H., Hills, J.H. and Azzorpardi, B.J., A Study of the Bubble-to-Slug Transition in Vertical Gas-Liquid Flow in Columns of Different Diameter, Int. J. Multiphase Flow, Vol.24, No.3, pp.431-452, 1998.

[14] Sun, B., Wang, R., Zhao, X. and Yan, D., The Mechanism for the Formation of Slug Flow in Vertical Gas-liquid Two-phase Flow, Solid-State Electronics, Vol.46, No.12, pp.2323-2329, 2002.

[15] Hout, R.V., Bernea, D. and Shemer, L., Evolution of Statistical Parameters of Gas-Liquid Slug Flow along Vertical Pipes, Int. J. Multiphase Flow, Vol.27, pp.1579-1602, 2001.

[16] Hout, R.V., Bernea, D. and Shemer, L., Evolution of Hydrodynamic and Statistical Parameters of Gas-Liquid Slug Flow along Inclined Pipes, Chemical Engineering Science, Vol.58, pp.115-133, 2003.

[17] Shemer, V., Hydrodynamic and Statistical Parameters of Slug Flow, International Journal of Heat and Fluid Flow, Vol.24, pp.334–344, 2003.
[18] Hout, R.V., Gulitski, A., Barnea, D. and Shemer, L., Experimental Investigation of the Velocity Field Induced by a Taylor Bubble Rising in Stagnant Water, International Journal of Multiphase Flow, Vol.28, No.4, pp.579-596, 2002.
[19] Ferziger, J.H. and Peric, M., Computational Methods for Fluid Dynamics, 3rd edition, Springer, Germany, 2002.
[20] Chapra, S.C. and Canale, R.P., Numerical Methods for Engineers, 3rd edition, McGraw-Hill, Singapore, 1998.
[21] White, E.T. and Beardmore, R.H., The velocity of rise of single cylindrical air bubbles through liquids contained in vertical tubes, Chemical Engineering Science, Vol.17, No.5, pp.351-361, 1962.